Fusion of TOF and TDOA for 3GPP Positioning

Kamiar Radnosrati, Carsten Fritsche, Gustaf Hendeby, Fredrik Gunnarsson†, Fredrik Gustafsson
Department of Electrical Engineering, Linköping University, Linköping, Sweden
Email: kamiar.radnosrati@liu.se, {carsten, hendeby, fredrik}@isy.liu.se
† Ericsson Research, Linköping, Sweden, Email: fredrik.gunnarsson@ericsson.com

***Abstract*—Positioning in cellular networks is often based on mobile-assisted measurements of serving and neighboring base stations. Traditionally, positioning is considered to be enabled when the mobile provides measurements of three different base stations. In this paper, we additionally investigate positioning based on time series of Time Of Flight (TOF) and Time Difference of Arrival (TDOA) measurements gathered from two base stations with known positions, where the specific base stations involved depend on the trajectory of the mobile station.. The set of two base stations is different along the trajectory. Each report contains TOF for the serving base station, and one TDOA measurement for the most favorable neighboring base station relative the serving base station. We derive explicit analytical solution related to the intersection of the absolute distance circle (from TOF) and relative distance hyperbola (from TDOA). We consider both geometric noise-free problem and the more realistic problem with additive noise as delivered in the 3rd Generation Partnership Project (3GPP) Long-Term Evolution (LTE). Positioning performance is evaluated using the Cramér-Rao lower bound.**

I. Introduction

Locating a Mobile Station (MS) by means of available cellular network resources is investigated in this paper. Among different available alternatives such as Angle of Arrival (AoA), Received Signal strength (RSS), Time of Flight (TOF) and Time Difference of Arrival (TDOA), this work focuses on the two latter measurements. The MS detects and measures the time of arrival of signals transmitted from cellular radio network Base Stations (BS)s that are separated spatially, and forms TDOA estimates. Hyperbolic positioning generally refers to TDOA localization where two involved stations form the foci of the hyperbola. In case of TOF measurements, the target would be located somewhere on a sphere or circle around the listening BS.

The accuracy horizon considered for 5th Generation (5G) networks according to recent studies is set to be within sub-meter bounds [1], [2]. It provides a considerably higher accuracy than other available alternatives. For instance, TDOA measurements provided by the 3GPP standard use Observed Time Difference of Arrival (OTDOA) techniques. Long Term Evolution (LTE) systems have an accuracy of a few tens of meters [3], [4]. Global Navigation Satellite Systems (GNSS)s, as another example, are limited to an accuracy of around 5m [5]. WLAN-based finger-printing systems are capable of providing around 4m-accurate solutions [6]. A whole survey regarding accuracies in different standards can be also found in [7], [8].

Different aspects of positioning using passive ranging measurements have already been analyzed in the literature. Closed-form solutions for hyperbolic positioning can be found for instance in [9]–[11]. Iterative algorithms for solving a nonlinear (weighted) least squares (N(W)LS) form another major group. The Gauss-Newton algorithm is studied in [12], constrained and non-constrained NLS solutions are discussed in [13], [14]. The iterative approaches generally require good initialization to converge to the global optimum of the cost function and often many iterations. In order to avoid these issues, the solutions proposed in [15], [16] transform nonlinear equations into a set of linear ones, thus making real-time implementations possible. Factor graph-based methods carrying low-complex flags also attracted some attention [17], [18].

The transmitted signal's waveform is known for transmitted pilot symbols, thus the receiver can measure range to any reference point by matching the signal with its delayed version. This is known as active localization method where availability of TOF measurements is guaranteed. In cooperative or semi-cooperative passive localization scenarios it is also possible to find TOF measurements at a single sensor as in [19].

It is often presumed in MS-assisted positioning that three different BSs must be measured in order to localize a target. The contribution of this work is to fuse TOF and TDOA measurements gathered from two BSs over a time series. The way how these measurements are obtained also matters. For example, [20] assumes reference sensors on fixed locations. In this work, BSs to which range is measured at each time instant change along the trajectory. The closest BS to the MS at each instant is taken for TOF and the most favorable neighboring BS relative the first one for TDOA.

The rest of the paper is organized as follows. Section II formulates the problem and introduces the motivation behind the work. Section III considers the noise-free case where first a scenario with three measured BSs is provided followed by a scenario with only two BSs. Section IV considers a more realistic situation where TOF and TDOA measurements are used for position estimation in the presence of additive Gaussian noise. Section V presents the result of the proposed estimator and the achieved positioning error, followed by the final conclusions in Section VI.

II. Motivation and Problem Formulation

Positioning in cellular radio networks is performed by processing position-dependent information contained in the signals the BS and the MS are exchanging with each other.

In cellular radio networks, the MS is generally assigned to a specific BS, the serving BS, which is responsible for the communication link with the MS; other BSs are referred to as neighboring BSs. The coverage area of each BS can be visualized by a hexagonally shaped cell, even though the actual coverage area depends on the actual radio propagation conditions, antenna configurations, transmission power in relation to neighboring cells. While the MS is moving through the network, it will be handed over to different cells, via a handover procedure. Their handover process is typically supported by event-triggered MS assisted measurements, indicating when a neighboring BS signal is measured at a better (with hysteresis) received strength compared to a signal from the serving BS.

While cellular radio networks were traditionally designed for communication purposes, its potential for positioning was soon realized [6]. For instance, timing measurements performed by the serving BS are used to ensure a proper alignment of the message frames required in time division multiple access (TDMA) based systems. The positioning accuracy in the early stages was rather poor, which was due to the fact that the used signals were not designed for positioning purposes. However, in recent years there has been a tremendous standardization effort, to increase this accuracy, which was also a result of FCC regulations on emergency calls that were established in the U.S.. Today's cellular radio networks standards enable the configuration of positioning reference signals (PRS) from BSs which enable MS to estimate TDOA measurements. In 3GPP LTE, these PRs can be defined based on orthogonal patterns, as well as muting schemes, where some BSs transmit a PRS, while other BSs are muted, in order to suppress interference and ensure a wide detectability of signals.

The purpose of the present work is to study the positioning performance in cellular radio networks that can be expected taking into account the above stated limitations. We assume that BSs are deployed in a cellular radio network consisting of hexagonal cells [4] and consider two different scenarios. The first scenario assumes that three BSs are involved in the positioning process as shown in Fig. 1. The serving BS S_1 is assumed to provide the TOF measurement, and two neighboring BSs S_2 and S_3 are detected by the MS to form TDOA measurements. The second scenario assumes that only two BSs are involved in the positioning process. Again, the serving BS S_1 is providing the TOF measurement, but now the TDOA is measured based on signals from the serving BS S_1 and a neighboring BS e.g. S_2. We further restrict ourselves to two-dimensional scenarios, and convert TOF and TDOA measurements to corresponding range and range differences. Geometrically, this means that the TOF measurement can be represented by a circle around the serving BS and the TDOA by a hyperbola with foci equivalent to the two neighboring BSs as depicted in Fig. 1. The MS positioning problem then becomes a classical circle and hyperbola intersection problem.

We further assume that the MS is moving on a predefined trajectory, which has a flower-shape structure as depicted in Fig. 2. The serving BS and the neighboring BSs involved in the positioning process will change depending on the current location of the MS. The flower shape of the trajectory is selected to excite key aspects of positioning based on TOF and TDOA. It can be a relevant reference scenario for comparative performance evaluations. The scenario data will be available for download online with the final version of the paper.

In order to simplify the analysis, we assume that the serving BS is the BS that has the smallest geometric distance to the MS. Similarly, the two neighboring BSs are defined to be the BSs which are geometrically the second and third closest to the MS. With these assumptions, it is possible to define areas identifying which BS is providing TOF measurements and which pair of BSs are detected for TDOA measurements as shown in Fig. 2a and Fig. 2b, respectively. Interestingly, the areas for TOF measurements define hexagonal cells, while the areas for the detected BS pairs for TDOA measurements define parallelograms (e.g. the area where BS S_1 and S_5 are detected for the TDOA measurement is defined as the parallelogram having corners defined by S_1 and S_5).

III. Geometric fusion of TOF and TDOA

We first consider the case where TOF and TDOA measurements are noise-free. While this case is of limited practical interest it is included here as it prepares the reader for the (more interesting) case of having noisy measurements which is presented in Section IV. Analytical solutions to the circle and hyperbola intersection problem can be derived for any BS deployment. However, assuming a deployment with hexagonal cells and BSs located at the centre of each cell as given in Fig. 1 together with an equivalent inter-site distance D between all cells (i.e. distance between two BSs is equal), the calculations can be considerably simplified. In particular, it is then possible to transform the problem into a local coordinate system (via translation and rotation) at each time instant the BSs involved in the positioning process change, and solve for the MS position in that local coordinate system.

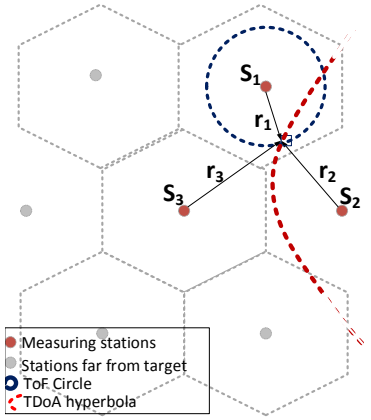

Fig. 1: Cellular radio network deployment and example for BS involved in the positioning process using TOF measurement from BS S_1 and TDOA measurements based on signals from BS S_2 and S_3.

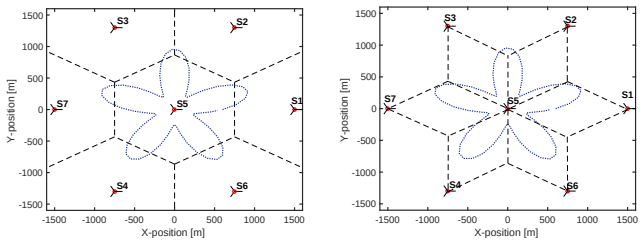

(a) TOF (b) TDOA

Fig. 2: Simulation scenario with flower-shaped MS trajectory, and areas identifying (a) which BS is providing TOF measurements, and (b) which pair of BSs is detected for TDOA measurements

Let $[X_i, Y_i]^T$, $i = 1, 2, 3$ denote the a priori known BS positions and let $[X, Y]^T$ denote the unknown MS position in some global coordinate system. We then transform the BS positions and MS position into some local coordinates given by $\mathbf{x}_i = [x_i, y_i]^T$ and $\mathbf{x} = [x, y]^T$.

A. Three Base Stations Scenario

The transformation of the three BSs scenario into a local coordinate system is depicted in Fig. 3. The local x-axis is chosen such that the two neighboring BSs S_2 and S_3, which are detected for the TDOA measurement (the focal points of the hyperbola), are located at $[\frac{D}{2}, 0]^T$ and $[-\frac{D}{2}, 0]^T$, respectively. The equal inter-site distance D then would imply that the serving BS S_1 providing TOF measurements is located at $[0, \frac{\sqrt{3}}{2}D]^T$. Further definitions of hyperbola related parameters given in this figure are the semi-major axis from the origin to each vertex, which is denoted by a, and the conjugate axis of the hyperbola which is then given by $2b$. Let r_1 denote

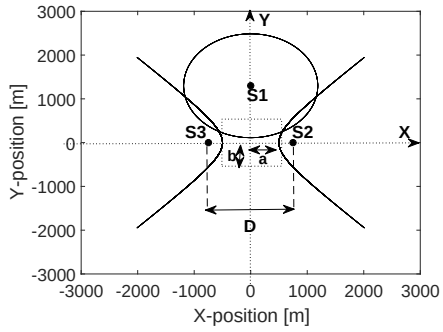

Fig. 3: Equivalent local coordinate system for the three BS scenario

the noise-free range corresponding to the TOF measurement of the serving BS, and let $r_{32} \triangleq r_3 - r_2$ denote the noise-free range difference related to the TDOA measurement of the neighboring BSs. Then, the solution of the circle and hyperbola intersection problem is equivalent to solving the following system of (nonlinear) equations for $[x, y]^T$

$$x^2 + (y - \frac{\sqrt{3}}{2}D)^2 = r_1^2, \tag{1a}$$

$$\frac{x^2}{a^2} - \frac{y^2}{b^2} = 1, \tag{1b}$$

where the parameters related to the semi-major and conjugate axis of the hyperbola are given by

$$a^2 = \frac{1}{4}r_{32}^2, \tag{2a}$$

$$b^2 = \frac{1}{4}(D^2 - r_{32}^2). \tag{2b}$$

Note, that according to (2a), two vertices of the hyperbola are located at $[-\frac{1}{2}r_{32}, 0]^T$ and $[\frac{1}{2}r_{32}, 0]^T$. This means that we generally have two hyperbolas and depending on how the range difference is defined (i.e. r_{32} or r_{23}) and whether the range difference is positive or negative, the MS must either lie on one of these. In Fig. 3, the MS position must lie on the hyperbola with BS S_2 as focal point, since $r_{32} > 0$. It is further worth noting that (2b) implies that $r_3 - r_2 < D$ must hold, but this is always satisfied based on our assumption stated at the end of Section II that $r_3 > r_2 > r_1$.

Mathematically, the intersection problem (1) has no, one or two solutions. However, considering how BSs are set, in the noise-free scenario, TDOA hyperbola will always intersect TOF circle. That is, in this setup the case with no solution never occurs. Constraints on either having one or two solutions depend on the geometric properties of BSs as well as their distance to the MS as given by

$$\mathbf{x} = \begin{cases} [x, y]^T, & \text{if } 0 < r_3 - r_2 < r_1, \\ [x_+, y_+]^T, & \text{if } r_3 - r_2 = r_1, \end{cases} \tag{3}$$

with

$$x = \frac{\sqrt{4D^4 r_{32}^2 - 7D^2 r_{32}^4 + 4D^2 r_{32}^2 r_1^2 \pm 4\sqrt{3}\theta}}{2D^2} \triangleq g_1(r_1, r_{32}), \tag{4a}$$

$$y = \frac{3D^4 r_{32}^2 - 3D^2 r_{32}^4 \pm 2\sqrt{3}\theta}{2\sqrt{3}D^3 r_{32}^2} \triangleq g_2(r_1, r_{32}), \tag{4b}$$

where

$$\theta = \sqrt{D^4 r_{32}^4 \left(r_{32}^2 - D^2\right)\left(r_{32}^2 - r_1^2\right)}. \tag{5}$$

B. Two Base Stations Scenario

The transformation of the two BSs scenario into a local coordinate system is depicted in Fig. 4. The local x-axis is chosen such that the serving BSs S_1 is located at $[D/2, 0]^T$ and the neighboring BS S_2 is located at and $[-D/2, 0]^T$. The noise-free range and range difference measurements are then defined as r_1 and $r_{21} \triangleq r_2 - r_1$, respectively. The solution of the circle and hyperbola intersection problem is equivalent

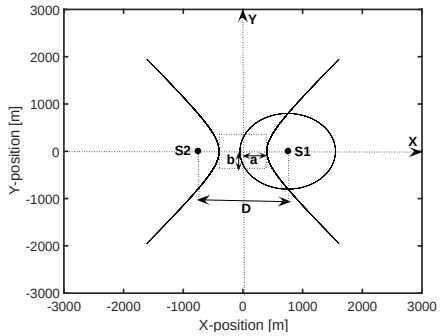

Fig. 4: Equivalent local coordinate system for the two BS scenario

to solving the following system of (nonlinear) equations for $[x, y]^T$

$$(x - \frac{D}{2})^2 + y^2 = r_1^2, \tag{6a}$$

$$\frac{x^2}{a^2} - \frac{y^2}{b^2} = 1, \tag{6b}$$

with $a^2 = \frac{1}{4}r_{21}^2$ and $b^2 = \frac{1}{4}(D^2 - r_{21}^2)$. Intersection points would then be dependent on the distance between two stations and r_1 as given by

$$\mathbf{x} = \begin{cases} [x, \pm y]^T & \text{if } D - 2r_1 < r_{21} < D \\ [x, 0]^T & \text{if } r_{21} = D - 2r_1 \end{cases} \tag{7}$$

with

$$x = \frac{r_{21}\left(r_{21} + 2r_1\right)}{2D} \triangleq g_1(r_1, r_{21}) \tag{8a}$$

$$y = \frac{\sqrt{(D^2 - r_{21}^2)\left(r_{21}^2 + 4r_{21}r_1 - D^2 + 4r_1^2\right)}}{2D} \triangleq g_1(r_1, r_{21}) \tag{8b}$$

IV. Stochastic fusion of TOF and TDOA

In this section we consider the more realistic assumption that the TOF and TDOA measurements are affected by noise. In particular we assume that the MS position solutions provided in the previous section are affected by measurements corrupted by additive noise. Let $\mathbf{z}$ denote the vector containing TOF and TDOA measurements. Further, let $\mathbf{e}$ denote the noise vector which is assumed Gaussian distributed $\mathbf{e} \sim \mathcal{N}(\bar{\mathbf{e}}, \mathbf{R})$ with mean $\bar{\mathbf{e}}$ and covariance matrix $\mathbf{R}$. The generic MS position solution provided in the previous section can be then expressed as $\mathbf{x} = [x, y]^T = \mathbf{g}(\mathbf{z} - \mathbf{e})$, where the mapping $\mathbf{g}(\mathbf{z}-\mathbf{e}) = [g_1(\mathbf{z}-\mathbf{e}), g_2(\mathbf{z}-\mathbf{e})]^T$ with $\mathbb{R}^2 \to \mathbb{R}^2$ nonlinearly relates the stochastic vector $(\mathbf{z}-\mathbf{e})$ to the MS position $\mathbf{x}$. Since the mapping $\mathbf{g}(\cdot)$ is nonlinear, the corresponding MS position will be non-Gaussian distributed. Hence, the MS position estimation problem can be casted into the problem of efficiently approximating the mean and covariance of Gaussian random variables that have been transformed through nonlinearities.

In the literature, there exist many different approaches that are suitable for the above estimation task, such as e.g. the sigma-point transformation or Monte Carlo transformation. In this work, we restrict our analysis to a first-order Taylor approximation of the nonlinear mapping $\mathbf{g}(\mathbf{z} - \mathbf{e})$ around the measurement vector $\mathbf{z}$, which we call first order Taylor transformation (TT1), yielding

$$\mathbf{x} = \mathbf{g}(\mathbf{z} - \mathbf{e}) \approx \mathbf{g}(\mathbf{z}) - \mathbf{g}'(\mathbf{z})\mathbf{e}, \tag{9}$$

where $\mathbf{g}'(\cdot)$ is the gradient of $\mathbf{g}(\cdot)$ with respect to $\mathbf{z}$. From this linear approximation, we obtain the mean and covariance which is sometimes referred to as Gauss' approximation formula, yielding

$$\boldsymbol{\mu}_{\mathbf{x}} = \mathbb{E}_{\mathbf{x}}(\mathbf{x}) \approx \mathbf{g}(\mathbf{z}) \tag{10a}$$

$$\mathbf{P}_{\mathbf{x}} = \mathrm{Cov}(\mathbf{x}) \approx \mathbf{g}'(\mathbf{z})\mathbf{R}\left(\mathbf{g}'(\mathbf{z})\right)^T \tag{10b}$$

In the following, we let $\hat{\mathbf{x}} = \boldsymbol{\mu}_{\mathbf{x}}$ denote our MS position estimator with corresponding estimation uncertainty given by covariance $\mathbf{P}_{\mathbf{x}}$.

A. Three Base Stations Scenario

For the three BSs scenario, the measurement vector is given by $\mathbf{z} = [z_1, z_{32}]^T$, where z_1 denotes the noisy range measurement from the serving BS S_1 and z_{32} denotes the noisy range difference measurement obtained from the neighboring BSs S_3 and S_2. The corresponding measurement models are of the following form

$$z_1 = r_1 + e_1 \tag{11a}$$

$$z_{32} = r_3 - r_2 + e_3 - e_2 \triangleq r_{32} + e_{32} \tag{11b}$$

where $e_1, e_2, e_3 \sim \mathcal{N}(0, \sigma^2)$, so that $e_{32} \sim \mathcal{N}(0, 2\sigma^2)$ and $\mathbf{R} = \mathrm{diag}([\sigma^2, 2\sigma^2])$. The position estimator $\hat{\mathbf{x}}$ is rather simple, as it only replaces the noise-free measurements r_1 and r_{32} by the noisy measurements $\mathbf{z}$ in the results provided in Section III-A. The computation of the estimator's covariance $\mathbf{P}_{\mathbf{x}}$ is rather cumbersome as it requires to compute the gradient matrix

$$\mathbf{g}'(z_1, z_{32}) = \begin{bmatrix} \frac{\partial g_1(z_1, z_{32})}{\partial z_1} & \frac{\partial g_1(z_1, z_{32})}{\partial z_{32}} \\ \frac{\partial g_2(z_1, z_{32})}{\partial z_1} & \frac{\partial g_2(z_1, z_{32})}{\partial z_{32}} \end{bmatrix}. \tag{12}$$

For the problem at hand, the matrix elements are generally available in closed-form, but are too lengthy to include here.

B. Two Base Stations Scenario

For the two BSs scenario, the measurement vector is given by $\mathbf{z} = [z_1, z_{21}]^T$, where z_{21} denotes the noisy range difference measurement obtained from the neighboring BS S_2 and serving BS S_1. The corresponding measurement model is given as follows

$$z_{21} = r_2 - r_1 + e_2 - e_1 \triangleq r_{21} + e_{21}, \tag{13}$$

where $e_{21} \sim \mathcal{N}(0, 2\sigma^2)$ and

$$\mathbf{R} = \begin{bmatrix} \sigma^2 & -\sigma^2 \\ -\sigma^2 & 2\sigma^2 \end{bmatrix}. \tag{14}$$

The position estimator $\hat{\mathbf{x}}$ is again only using noisy measurements instead of noise-free measurements in the solutions

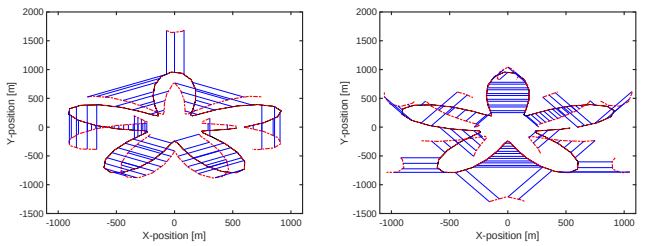

(a) (b)

Fig. 5: Illustration of position ambiguity from the geometric solution. (a) Two involved BSs, (b) Three involved BSs

provided in Section III-B. The gradient matrix $\mathbf{g}'(z_1, z_{21})$ for the two BS scenario when $[x, y]^T$ is the solution, is then given by

$$\begin{bmatrix} \frac{z_{21}}{D} & \frac{z_1+z_{21}}{D} \\ \frac{\left(D^2-z_{21}\right)^2(2z_1+z_{21})}{D\delta} & \frac{\left(D^2-z_{21}\right)\left(D^2(2z_1+z_{21}+1)-2(z_1+z_{21})(2z_1+z_{21})\right)}{2D\delta} \end{bmatrix} \tag{15}$$

where $\delta = \sqrt{\left(D^2 - z_{21}\right)^2\left((2z_1 + z_{21})^2 - D^2\right)}$. The second row in (15) must be multiplied by -1 when the solutions is $[x, -y]^T$.

V. Simulation Result

The proposed TT1 estimators introduced in Section IV can be applied to any generic setup of BSs as long as the the inter-site distance D is the same for all BSs. In order to assess the analytical position solutions of the noise-free measurement, we compute these for each point on the flower shape trajectory being covered by seven BSs as described in Section II. The moving MS reports ranging measurements to involved BSs. The measuring BSs are defined by their distance to the target and are not fixed throughout the whole trajectory.

At each time instant, we first transform the global coordinates to a local coordinate system for which solutions have been provided in Section III. The estimated position is then transformed back to the global coordinates for positioning performance metric computations. Fig. 5 illustrates that most of the time there are two solutions at each position along the trajectory for noise-free measurements, and that the incorrect positions seem to be mirror positions defined by the geometry of the scenario.

In order to evaluate the performance of the TT1 estimator, we calculate the root mean square error (RMSE) of the estimator. For the measurement noise standard deviation, we assume a value of $\sigma = 8.5$ m, which coincides with the value used in 3GPP-LTE systems [4]. For a number of N Monte Carlo runs, the RMSE is defined as

$$\text{RMSE} = \sqrt{\frac{1}{N}\sum_{i=1}^{N}(\hat{x}_i - x)^2 + (\hat{y}_i - y)^2}, \tag{16a}$$

where $[\hat{x}_i, \hat{y}_i]^T$ corresponds to the estimated MS position at the i-th Monte Carlo run and $[x, y]^T$ is the true position. We consider the true positions as prior information in cases when two solutions exist. The prior information is used by the estimator to select the position solution that minimizes the L_2 norm between true position and that point. In this way, we avoid the position ambiguity and evaluate only the stochastic contribution to the position error. In a real scenario, however, the position prior shall be provided by a tracking filter. For all simulations we have performed $N = 500$ Monte Carlo runs.

Fig. 6b corresponds to the scenario with three measured BSs. As it is shown, the positioning error along the trajectory varies between 11 to 18 meters by using TT1 estimator and measuring three BSs. The Cramér-Rao lower bound (CRLB) for this scenario is also plotted to represent the lower bound to be achieved.

Fig. 6a represents the RMSE and the CRLB when two BSs are measured. As expected, it has less accuracy than the case with three BSs. Additionally, there are seven regions where the estimation error is much larger, and is of the magnitude of one hundred. These points correspond to the geometry of , which can be easily mitigated with a tracking filter. Thus, a tracking filter has a large potential to assist the snapshot estimate as studied in this contribution, and this is the subject for future work.

Scatter plots of the estimated positions using the proposed TT1 estimator along the trajectory are presented in Fig. 6c for the two BSs scenario and in Fig. 6d for the three BSs scenario. It is interesting to note that there is always at least one solution in case we assume noise-free measurements. However, this is generally not true when having noisy measurements. The Gaussian noise may result in smaller TOF circles or shifted TDOA hyperbolas. In the noise-free measurement case having only one solution corresponds to the case when the hyperbola touches the circle at a single point. In this case, having a unfavorable noise realization might move the hyperbola outside the circle so that there is no intersection at all. This occurred a couple of times in both scenarios. There is a natural estimate in such cases, namely the geometric solution that gives the point closest to both the circle and hyperbola, which is subject to further research.

VI. Conclusions

Fusion of TOF and TDOA measurements systems for positioning purposes has been investigated in this paper. The problem formulation is inspired by a recent standardization decision in 3GPP-LTE, which will make these type of measurements available with rather good accuracy. The analytical solution to the intersection of the circle and hyperbola coming from two measurements together with constraints of the solution are provided. While the MS moves around the trajectory the known reference points change depending on the distance to the MS. Two scenarios are investigated in which the number of known BSs is different. In the first scenario, the MS provides periodic reports to three different BSs while in the second scenario, positioning is performed by measuring

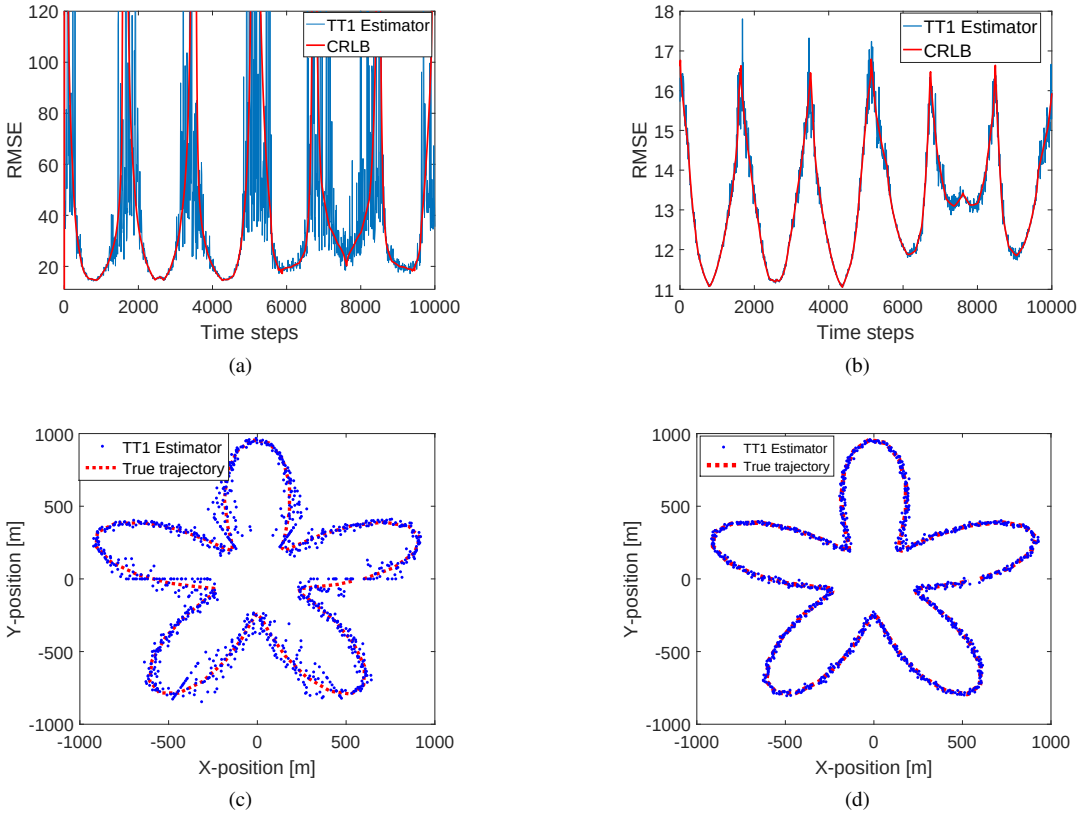

Fig. 6: Positioning error and estimated trajectory Left column, Two involved BSs, Right column Three involved BSs

only two BSs. We propose an estimator based on a Taylor approximation of the non-linear mapping between TOF and TDOA measurements and the 2D position of the MS. Monte Carlo simulations indicate good performance that is close to the CRLB for both scenarios.

VII. Acknowledgement

This work is funded by the European Union FP7 Marie Curie training program on Tracking in Complex Sensor Systems (TRAX).

References

[1] 5G Forum, "5G white paper: New wave towards future societies in the 2020s,," March 2015.

[2] N. Wood, "Japan, Korea in 5G one-upmanship," June 2015, Total Telecom.

[3] J. Medbo, I. Siomina, A. Kangas, and Furuskog, "Propagation channel impact on LTE positioning accuracy: A study based on real measurements of observed time difference of arrival," Personal, Indoor and Mobile Radio Communications, 2009 IEEE 20th International Symposium on. Tokyo, Japan.: IEEE, 13-16 Sep. 2009, pp. 2213–2217.

[4] H. Ryden, S. Modarres Razavi, F. Gunnarsson, S. M. Kim, M. Wang, Y. Blankenship, G. A., and A. Busin, "Baseline performance of LTE positioning in 3GPP 3D MIMO indoor user scenarios," Localization and GNSS (ICL-GNSS), International Conference on. Gothenburg, Sweden.: IEEE, 1-6 Jun. 2015, pp. 1–6.

[5] D. Dardari, P. Closas, and Djuric, "Indoor tracking: Theory, methods, and technologies," *IEEE Transactions on Vehicular Technology*, vol. 64, no. 4, pp. 1263–1278, April 2015.

[6] H. Liu, Y. Gan, J. Yang, S. Sidhom, Y. Wang, Y. Chen, and F. Ye, "Push the Limit of WiFi Based Localization for Smartphones,." Istanbul, Turkey.: Proceedings of the 18th Annual International Conference on Mobile Computing and Networking, 22-26 Aug. 2012, pp. 306–316.

[7] F. Gustafsson and F. Gunnarsson, "Mobile positioning using wireless networks: Possibilities and fundamental limitations of positioning using wireless communications networks," *IEEE Signal Processing Magazine*, vol. 22, no. 4, pp. 41–53, Jul. 2005.

[8] K. Radnosrati, F. Gunnarsson, and Gustafsson, "New trends in radio network positioning," Information Fusion (Fusion), 18th International Conference on. Washington, D.C, USA.: IEEE, 6-9 Jul. 2015, pp. 492–498.

[9] Y. T. Chan and K. C. Ho, "A simple and efficient estimator for hyperbolic location," *IEEE Transactions on Signal Processing*, vol. 42, no. 8, pp. 1905–1915, Aug. 1994.

[10] M. D. Gillette and Silverman, "A linear closed-form algorithm for source localization from time-differences of arrival," *IEEE Signal Processing Letters*, vol. 15, pp. 1–4, Jan. 2008.

[11] H. C. So, Y. T. Chan, and F. K. W. Chan, "Closed-form formulae for time-difference-of-arrival estimation," *IEEE Transactions on Signal Processing*, vol. 56, no. 6, pp. 2614 – 2620, Jun. 2008.

[12] J. J. Caffery, *Wireless Location in CDMA Cellular Radio Systems*. Kluwer, 1999.

[13] J. Caffery and Stuber, "Subscriber location in cdma cellular networks," *IEEE Transactions on Vehicular Technology*, vol. 47, no. 2, pp. 406–416, May. 1998.

[14] K. W. Cheung, H. C. So, W.-K. Ma, and Y. T. Chan, "A constrained least squares approach to mobile positioning: Algorithms and optimality," *EURASIP J. Appl. Signal Process.*, vol. 2006, pp. 1–23, Jan. 2006.

[15] Y. Huang, J. Benesty, G. W. Elko, and R. M. Mersereati, "Real-time passive source localization: a practical linear-correction least-squares approach," *IEEE Transactions on Speech and Audio Processing*, vol. 9, no. 8, pp. 943–956, Nov. 2001.

[16] L. Cong and Zhuang, "Hybrid TDOA/AOA mobile user location for wideband CDMA cellular systems," *IEEE Transactions on Wireless Communications*, vol. 1, no. 3, pp. 439–447, Jul. 2002.

[17] J. Chen, Y. Maa, C.S. Wang, and J. Chen, "Mobile position location using factor graphs,," *IEEE COMMUNICATIONS LETTERS*, vol. 7, no. 9, pp. 431–433, Sep. 2003.

[18] C. Mensing and S. Plass, "TDoA positioning based on factor graphs," The 17th Annual IEEE International Symposium on Personal, Indoor and Mobile Radio Communications (PIMRC06). Helsinki, Finland: IEEE, 11-14 Sep. 2006, pp. 1–5.

[19] C. Steffes, R. Kaune, and S. Rau, "Determining times of arrival of transponder signals in a sensor network using GPS time synchronization." Berlin, Germany: Informatik, Workshop Sensor Data Fusion: Trends, Solutions, Applications,, 4-7 Oct. 2011.

[20] T. Sathyan, M. Hedley, and Mallick, "An analysis of the error characteristics of two time of arrival localization techniques," Information Fusion (FUSION),13th Conference on. Edinburgh, UK.: IEEE, 26-29 Jul. 2010, pp. 1–7.